

Strong terahertz emission from superlattices via Zener tunneling

Peng Han, Kui-juan Jin,^{*} Yue-liang Zhou, Hui-bin Lu, and Guo-zhen Yang

*Beijing National Laboratory for Condensed Matter Physics,
Institute of Physics, Chinese Academy of Sciences, Beijing 100080, China*

Barry C. Sanders

*Institute for Quantum Information Science,
University of Calgary, Calgary, Alberta T2N 1N4, Canada and
Centre for Quantum Computer Technology,
Macquarie University, Sydney, New South Wales 2109, Australia*

Abstract

We develop a comprehensive, elegant theory to explain terahertz (THz) emission from a superlattice over a wide range of applied electric field, which shows excellent agreement between theory and experiment for a GaAs/Al_{0.3}Ga_{0.7}As superlattice. Specifically we show that increasing electric field increases THz emission for low fields, then reduces emission for medium fields due to field-induced wave function localization, and then increases emission in the high field due to delocalization and Zener tunneling between minibands. Our theory shows that Zener tunneling resonances yield high THz emission intensities and points to superlattice design improvements.

PACS numbers: 73.21.Cd, 73.40.-c, 78.47.+p

The immense value of coherent terahertz (THz) electromagnetic radiation in many fields, including medical imaging, molecule recognition, sub-millimeter astronomy, remote sensing, and condensed matter physics¹, has provided the impetus for vigorous research efforts into creating new sources of reliable and affordable THz radiation^{2,3} including exploiting Bloch oscillations in a superlattice (SL)⁴. The SL is especially promising as a THz source because it is effectively an artificially engineered semiconductor with tunable parameters and is thus adaptable. Vigorous experimental research^{5,6,7,8} has been accompanied by theoretical advances^{9,10,11}, but a proper theory that explains the physics and the THz emission properties for a SL THz source over a wide range of electric field has been elusive until now.

We present a quantitative theory that explains THz emission from a SL over a wide range of applied electric field, and our theory also explains qualitatively the rise and fall of emitted THz field intensity in the low field (LF) regime, the rise of emission in the medium field (MF) to high field (HF) regime, anomalous resonances observed in THz emission from a GaAs/Al_{0.3}Ga_{0.7}As SL⁸, and provides insight into the limitations in the ultrahigh field (UF) regime. Our theory elucidates the subtle physics of electromagnetic radiation emission in a SL subjected to high electric fields and, moreover, shows that Zener tunneling between minibands in the conduction band can be valuable especially for superior design of THz sources.

Usually theories consider SL behavior in the regime of weak applied electric field where Zener tunneling (typically deleterious, such as electrical breakdown in semiconductors due to tunneling to higher bands¹²), can be ignored⁹. However recently we have seen an indication that Zener tunneling between minibands of the conduction band¹⁰ coincide with the anomalous THz resonances observed in a GaAs/Al_{0.3}Ga_{0.7}As SL⁸. Inspired by this promising connection between theoretical enhanced Zener tunneling rates and observed THz resonances in a SL, we have developed a theory for THz emission from a SL subjected to a range of applied electric field; our theory explains experimental observations and provides a promising foundation from which to design SLs as versatile THz emitters.

We analyze THz emission intensity I from a SL in an electric field F by subdividing the behavior into four regimes of applied electric field: (i) the LF regime corresponds to I increasing for increasing applied electric field F ; (ii) the MF regime for which I decreases with increasing F ; (iii) the HF regime for which I again increases with increasing F and also demonstrates resonances; and (iv) the UF regime (with I decreasing with increasing F). Pre-

viously regimes (i) and (ii) have been separately explained by considering a single miniband within the conduction band using a Drude model for regime (i) and a quantum description for regime (ii)⁹; later the Kane model involving coupled Schrödinger equations¹³ was used to describe the cross-over between regimes (i) and (ii)¹⁴. More recently the locations of resonances in regime (iii) were identified with enhanced Zener tunneling rates between two minibands within the conduction band¹⁰ but the characteristics of I vs F were not presented. Here we present a full and complete theory for regimes (i-iii) that includes all the successes of these prior models and, furthermore, easily describes all the cross-overs between applied electric field regimes, shows excellent quantitative agreement especially at the resonances. Our perturbative two-miniband theory provides a clear intuitive understanding of THz emission from a SL in terms of localization of wave functions and properties of both minibands.

In our model the SL growth direction is along the x -axis with F in the positive x direction. For a and b the widths of the well and barrier, respectively, m the total number of unit cells (one well plus one barrier), $d = a + b$ the unit cell width (and the potential V periodic over width d), and \hbar the reduced Planck's constant, the Hamiltonian for an electron $-e$ and effective mass μ is

$$H = -\frac{\hbar^2}{2\mu} \frac{d^2}{dx^2} + V(x) + eFx, \quad V(x) = V(x + ld). \quad (1)$$

The spectrum is subdivided into minibands indexed by n , and we are interested in the case of two minibands so $n \in \{1, 2\}$. The eigenfunctions for $F = 0$ can be expressed as Bloch functions $\{\phi_{nk}(x)\}$, with corresponding eigenvalues $\{E_{nk}\}$ and Bloch number k in the Brillouin Zone (BZ). The Bloch functions and the eigenvalues in the SLs are obtained by using the Kronig-Penney model¹⁵ with a step size of $d/200$ and the BZ is sampled by 2000 points. In order to appreciate the role of inter-miniband tunneling, we study the system with Zener tunneling between minibands treated by perturbation theory; exact and numerical methods for solving Hamiltonian H (1) tend to obscure the important role played by tunneling. Furthermore we will see that the ultrahigh electric field regime, which is characterized by decreasing I , is where second-order perturbation effects become important.

The Bloch functions can be used as a basis set for $F \neq 0$ as well. In this case, a wave function confined to band n is $\Phi_{nl}(x) = \sum_{k \in \text{BZ}} a_{nlk} \phi_{nk}(x)$, with the coefficients $\{a_{nlk}\}$ satisfying a well known relation^{16,17}. Inter-miniband tunneling is calculated via dual degen-

erate perturbation theory. The zeroth-order wave function $\psi_{1l,2l'}^{(0)}(x) = C_{1l}\Phi_{1l}(x) + C_{2l'}\Phi_{2l'}(x)$ straddles both minibands, with l' satisfying the condition that the energy difference $|\epsilon_{2l'} - \epsilon_{1l}|$ is minimized in $l' \in \{1, \dots, m\}$, and

$$\begin{pmatrix} H'_{1l,1l} & H'_{1l,2l'} \\ H'_{2l',1l} & H'_{2l',2l'} \end{pmatrix} \begin{pmatrix} C_{1l} \\ C_{2l'} \end{pmatrix} = \varepsilon_{1l}^{(1)} \begin{pmatrix} C_{1l} \\ C_{2l'} \end{pmatrix} \quad (2)$$

with $\varepsilon_{1l}^{(1)}$ the eigenvalue for first-order perturbation of Eq. (1) and $H'_{1l,2l'} = \langle \Phi_{1l}(x) | eFx | \Phi_{2l'}(x) \rangle$ the perturbation matrix element. The first-order wave function is

$$\begin{aligned} \psi_{1l,2l'}^{(1)}(x) = \sum_{l'' \neq l} \frac{\langle \psi_{1l'',2l'-l+l''}^{(0)}(x) | eFx | \psi_{1l,2l'}^{(0)}(x) \rangle}{\varepsilon_{1l}^{(0)} - \varepsilon_{1l''}^{(0)}} \\ \times \psi_{1l'',2l'-l+l''}^{(0)}(x), \end{aligned} \quad (3)$$

with $l'' \in \{1, \dots, m\}$ and $\varepsilon_{1l}^{(0)}$ the zeroth order eigenvalue. In the case of weak tunneling ($C_{1l} \rightarrow 1$, $C_{2l'} \rightarrow 0$), degenerate perturbation theory merges with non-degenerate perturbation theory. For first-order perturbation theory, the total wave function is $\psi_{1l,2l'}(x) = \psi_{1l,2l'}^{(0)}(x) + \psi_{1l,2l'}^{(1)}(x)$. We also perform the calculation to second order in order to separate first-order effects, which yield desirable resonances, and second-order effects, which we show limit performance in the ultrahigh-field regime. Whether the wave function $\psi_{1l,2l'}(x)$ is calculated to first- or second-order will be clear from the context.

We plot $\text{Re}[\psi_{1l,2l'}(x)]$ in Fig. 1 for several values of F to depict characteristics of this wave function such as localization and overlap with the nearest levels in each of the four F regimes (LF, MF, HF, UF). We see that the wave function can be localized or delocalized and may be confined to one miniband or overlap two minibands, with these characteristics important for understanding THz emission.

THz emission intensity depends on the wave function $\psi_{1l,2l'}(x)$ and on the applied electric field. The relationship between THz emission frequency ω_B and field strength F is given by $\hbar\omega_B = eFd$, which is the energy level splitting in the miniband. To calculate the total radiative intensity, we adapt the relation⁹

$$F \sum_{l''=1}^m |l - l''| \left| \int_{\text{SL}} dx \psi_{1l,2l'}^*(x) x \psi_{1l'',2l'-l+l''}(x) \right|^2 \quad (4)$$

to include broadening due to scattering; here $l \in \{1, \dots, m\}$, l' minimizes $|\varepsilon_{2l'}^{(0)} - \varepsilon_{1l}^{(0)}|$, and the wave functions implicitly depend on F . For the experiment to be considered in the

present paper, the energy half width of the pumping laser pulses is approximately 20 meV. Within this energy interval, the levels in the Wannier-Stark ladders (WSLs) are populated with equal probability⁹. Thus the summation runs over all pairs of WSL eigenfunctions.

It has been demonstrated in Ref.^{18,19} that the acoustical phonon scattering plays a decisive role in the THz radiation process. Let $|n, \vec{\rho}\rangle$ be the eigenstate of the n th WSL level, where $\vec{\rho}$ is the two-dimensional (2D) wave vector. As shown in Ref.¹⁸, in the steady state the electron population on each WSL level is the same, and there will be no net stimulated emission from the SLs due to the vertical transition from the initial state $|n + 1, \vec{\rho}\rangle$ to the final state $|n, \vec{\rho}\rangle$ is perfectly canceled by the absorption transition from state $|n, \vec{\rho}\rangle$ to state $|n + 1, \vec{\rho}\rangle$ that occurs at the same frequency and intensity without the effect of electron-phonon scattering⁹. However, in the transition processes involve the emission or absorption of an acoustical phonon, the in-plane momentum of the initial state will differ from that of the final state. Hence, the emitted THz radiation will not be completely reabsorbed by the

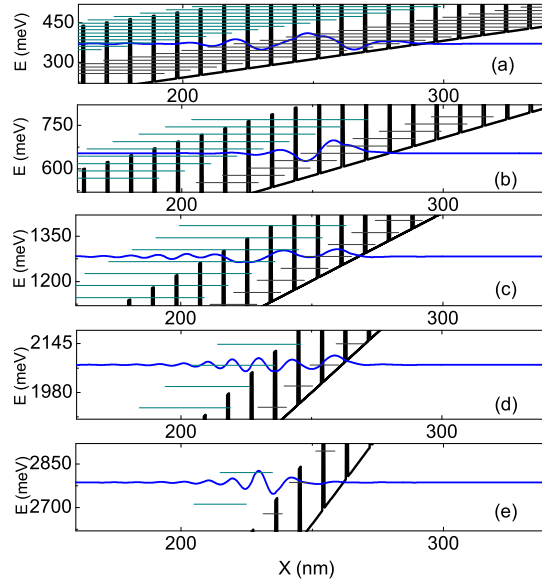


FIG. 1: (Color on-line) Plot of $\text{Re}[\psi_{1l,2l'}(x)]$ (blue line), which is the wave function at energy l, l' for applied electric field values (a) $F = 14\text{kV/cm}$ (LF), (b) $F = 26\text{kV/cm}$ (MF), (c) $F = 45\text{kV/cm}$ (HF away from THz resonance), (d) $F = 90\text{kV/cm}$ (HF near THz resonance), and (e) $F = 120\text{kV/cm}$ (UF). The horizontal lines are the equally spaced energy levels in each of the two minibands (right for the 1st miniband and left for the 2nd miniband).

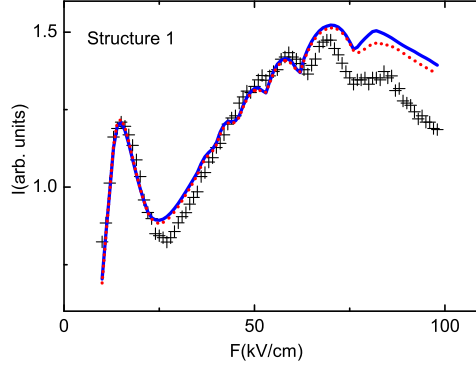


FIG. 2: (Color on-line) First-order (solid line) and second-order (dashed line) perturbation theory results vs experimental data [8] (black crosses) for structure 1.

system, and the system can have a net gain for the photon energy $\hbar\omega < \hbar\omega_B$. Because the energy of an acoustical phonon is much less than the energy of THz photon, we still treat the $\hbar\omega_B$ as the THz radiation photon energy in this work⁹.

Our theory is compared with recent experimental results on two GaAs/Al_{0.3}Ga_{0.7}As SL structures⁸: structure 1, $a = 6.4\text{nm}$ and $b = 0.56\text{nm}$ with $m = 73$ (first miniband: 18 to 114 meV; second miniband: 150 to 445 meV) vs structure 2, $a = 8.2\text{nm}$ and $b = 0.8\text{nm}$ with $m = 55$ (first miniband: 19 to 69 meV; second miniband: 107 to 270 meV). We show our calculated $I(F)$ characteristic for both first- and second-order perturbation theory in Figs. 2 and 3 alongside corresponding experimental results for both structures.

Two fitting parameters are used in our calculations to match theoretical and experimental curves: $I_\ell^{\text{plot}}(F) = \varsigma_0 I_\ell^{\text{calc}}(F) + \varsigma_1$, with I_ℓ^{plot} the plotted I for structure ℓ , I_ℓ^{calc} the calculated I , and the fitting parameters ς_0 for rescaling and ς_1 for background. The choice of both coefficients is jointly determined by least squares fitting for both sets of experimental data, with excellent agreement between second-order perturbation theory and experiment. First-order perturbation results agree for all electric field regimes except UF, thus revealing the important role of second-order effects in limiting achievable THz intensity.

Theoretical and experimental radiation intensities $I(F)$ are depicted in Figs. 2 and 3 for structures 1 and 2, with the theoretical curve determined by first- and second-order perturbation based on Eq. (4). As expression (4) ignores scattering, we incorporate the broadening effects by convolving $I(F)$ with a Lorentzian of half-width Γ , which is obtained based on

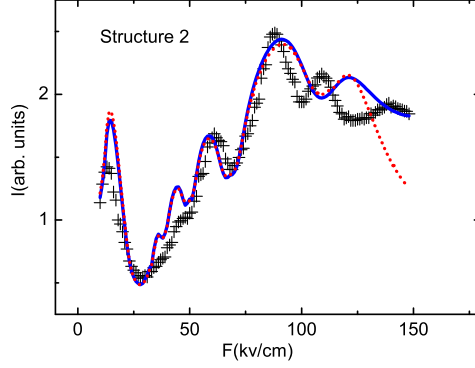


FIG. 3: (Color on-line) First-order (solid line) and second-order (dashed line) perturbation theory results vs experimental data [8] (black crosses) for structure 2.

TABLE I: Fitting parameters for structure 1 and 2

Parameters	ς_0	ς_1
Structure 1 (1st-order)	3.667	0.316
Structure 1 (2nd-order)	3.739	0.332
Structure 2 (1st-order)	2.598	0.164
Structure 2 (2nd-order)	2.771	0.134

the calculation of longitudinal optical phonon scattering^{20,21,22}, aluminum atom alloy scattering^{23,24} and interface roughness scattering^{25,26} by using Fermi's golden rule. Theory and experiment agree well for all field regimes except UF, and first-order perturbation results also agree for all applied field regimes except the UF. However note that the theoretical curve for structure 2 diverges somewhat from the UF intensity peaks of the experimental curve, which we believe is due to these two peaks arising from Zener tunneling between the second and third minibands; furthermore this anomaly is compounded by our least square fitting parameters ς_0 , and ς_1 truncated for $F_{\text{cut}} = 100$ and $F_{\text{cut}} = 120$ kV/cm for structure 1 and 2, respectively. The fitting parameters for the first-order and second-order perturbation calculation in structure 1 and 2 are given in table I.

The curves clearly exhibit four regimes of behavior according to the strength of the applied

electric field. We see that $I(F)$ rises monotonically for LF, then decreases monotonically in MF, and HF is characterized by a trend of I increasing with rising F but punctuated by resonances. Finally there is a region in the UF case with the experimental result for I decreasing with increasing F , which agrees with the second-order perturbation theory result, but disagreeing with first-order perturbation result. Our theory explains all these features as exemplified by Figs. 1. In Figs. 1(a,b), corresponding to the low- and medium-field regimes, respectively, the slopes of the minibands are small, and Zener tunneling between minibands can thus be ignored. In these two cases the wave functions are confined to the lowest miniband, but in (a) the function progressively spreads out with increasing F whereas it progressively localizes with increasing F (due to competition between localized wave functions) in (b)^{9,14}.

The HF regime in Figs. 1(c-d) exhibits clear effects due to inter-miniband tunneling. Fig. 1(c) shows steeper minibands than in 1(a-b), which causes the wave function to overlap both minibands. Analogous to (a), the wave function progressively spreads as F increases, yielding increasing THz emission with increasing F . However this increasing I with increasing F is punctuated with resonances due to Zener tunneling (this connection was speculated when coincidences between values of F values for enhanced Zener tunneling and experimentally observed resonances were demonstrated¹⁰).

Here we see exactly what is happening at the resonance: the wave function is localized in both minibands but with significant overlap, which is helped by alignment of the WSLs in each miniband, and hence are strongly coupled leading to enhanced THz emission. Increasing F partially leads to further localization, as in the medium-field regime, but causes the WSLs to become misaligned, thereby decreasing the Zener tunneling rate and causing a decrease of I with increasing F . In this way, we can understand the existence of these THz resonances, and, moreover, design SLs to exploit these emission peaks; moreover our theory makes it evident that, when second-order perturbation events become non-negligible, wave functions become progressively delocalized thereby making the SL an increasingly poor THz emitter.

In summary we have developed a clear model of electromagnetic emission from a SL, based on single miniband dynamics in the low- and medium-field regimes, and two-miniband dynamics in the high- and ultrahigh-field regimes. Our results contain previous theories for low- and medium-field dynamics as special cases and explain the coincidence of enhanced

Zener tunneling rates and experimentally-observed THz emission peaks. We have excellent quantitative agreement with experiment, subject to choosing two fitting parameters by using least squares fitting method, and we have a clear explanation of when and why THz emission becomes poor in the ultrahigh applied electric field regime. In addition to the value of our model as a design tool for SL THz emitters, our perturbation theory approach is remarkably successful in explaining electromagnetic radiation features in recent SL experiments due to confinement or coupling between minibands within the conduction band. Our approach also underscores the value of a perturbation theory approach, as opposed to exact or numerical means, to understand the underlying physics.

Acknowledgments

We gratefully acknowledge financial support from the National Natural Science Foundation of China (No. 60321003) and National Basic Research Program of China, and BCS also acknowledges support from iCORE, NSERC, and CIAR.

* Electronic address: kjjin@aphy.iphy.ac.cn

¹ D. M. Mittleman, M. Gupta, R. Neelamani, R. G. Baraniuk, J. V. Rudd, and M. Koch, et al, Appl. Phys. B: Laser Opt. **68**, 1085 (1999); K. Sakai, *Terahertz Optoelectronics* (Springer-Verlag, Berlin, 2005).

² N. Sekine, K. Yamanaka, K. Hirakawa, M. Voßebürger, P. Haring-Bolivar, and H. Kurz, et al, Appl. Phys. Lett. **74**, 1006 (1999); N. Sekine, K. Hirakawa, M. Voßebürger, P. Haring-Bolivar, and H. Kurz, et al, Phys. Rev. B **64**, 201323 (2001).

³ R. Ascazubi, I. Wilke, K. Denniston, H. Lu, and W. J. Schaff, et al, Appl. Phys. Lett. **84**, 4810 (2004).

⁴ C. Waschke, H. G. Roskos, R. Schwedler, K. Leo, H. Kurz, and K. Köhler, et al, Phys. Rev. Lett. **70**, 3319 (1993).

⁵ K. Leo, P. Haring-Bolivar, F. Brüggemann, R. Schwedler and K. Köhler, et al, Solid State Commun. **84**, 943 (1992).

⁶ K. Leo, *High-Field Transport in Semiconductor Superlattices* (Springer-Verlag, Berlin, 2003).

- ⁷ Y. Shimada, K. Hirakawa, and S.-W. Lee, Appl. Phys. Lett. **81**, 1642 (2002); Y. Shimada, K. Hirakawa, M. Odnoblioudov, and K. A. Chao, et al, Phys. Rev. Lett. **90**, 046806 (2003).
- ⁸ Y. Shimada, N. Sekine, and K. Hirakawa, Appl. Phys. Lett. **84**, 4926 (2004).
- ⁹ K.-j. Jin, M. Odnoblyudov, Y. Shimada, K. Hirakawa, and K. A. Chao, et al, Phys. Rev. B **68**, 153315 (2003).
- ¹⁰ P. Han, K.-j. Jin, Y. L. Zhou, Q.-l. Zhou, H.-b. Lu, D.-y. Guan and G.-z. Yang, et al, Europhys. Lett. **72**, 1011 (2005).
- ¹¹ A. Vojvodic, A. Blom, Zhongshui Ma, Y. Shimada, K. Hirakawa, and K. A. Chao, et al, Solid State Comm. **136**, 580 (2005).
- ¹² C. Zener, Proc. R. Soc. Lond. A, **145**, 523 (1934).
- ¹³ E. O. Kane, J. Phys. Chem. Sol. **12**, 181 (1959).
- ¹⁴ P. Han, K.-j. Jin, Y.-l. Zhou, and Q.-l. Zhou, Int. J. Mod. Phys. B **20**, 937 (2006).
- ¹⁵ S.-h. Pan, S.-m. Feng, Phys. Rev. B **44**, 5668 (1991).
- ¹⁶ W. V. Houston, Phys. Rev. **57**, 194 (1940).
- ¹⁷ S. Glutsch, Phys. Rev. B **69**, 235317 (2004).
- ¹⁸ B. Bastard and R. Ferreira, C. R. Acad. Sci. (Paris) **312**, 971 (1991).
- ¹⁹ Yu. A. Tarakanov, M. A. Odnoblyudov, K. A. Chao, N. Sekine, and K. Hirakawa, Phys. Rev. B **74**, 125321 (2006).
- ²⁰ P. Harrison, *Quantum wells, wires and dots* (Wiley, West Sussex, 2005).
- ²¹ Yu. A. Tarakanov, V. Vettchinkina, M. A. Odnoblyudov, K. A. Chao, N. Sekine, and K. Hirakawa, et al, Phys. Rev. B **72**, 125345 (2005).
- ²² P. Y. Yu and M. Cardona, *Fundamentals of Semiconductors*, 3rd ed. (Springer-Verlag, Berlin, 2003).
- ²³ P. Ray and P. K. Basu, Phys. Rev. B **45**, 9169 (1992).
- ²⁴ J. F. Palmier and A. Chomette, J. Phys. (Paris) **43**, 381 (1982).
- ²⁵ I. Dharssi and P. N. Butcher, J. Phys. Condens. Matter **2**, 4629 (1990).
- ²⁶ T. Unuma, N. Sekine, and K. Hirakawa, Appl. Phys. Lett **89**, 161913 (2006).